# Focal Mechanisms of the March 6, 1987 Ecuador Earthquakes —CMT Inversion with a First Motion Constraint—

Hitoshi Kawakatsu[1,*] and Gastón Proaño Cadena[2,**]

[1] Geological Survey of Japan, Tsukuba 305, Japan
[2] Building Research Institute, Tsukuba 305, Japan

For a shallow earthquake, $M_{r\theta}$ and $M_{r\phi}$ components of a moment tensor are difficult to constrain using long-period data only (Kanamori and Given, 1981). Many researchers have attempted to circumvent this difficulty by incorporating either first motion polarity data (e.g., Nakanishi and Kanamori, 1984; Michael and Geller, 1984; Tanimoto and Kanamori, 1986; Suetsugu and Nakanishi, 1988) or shorter-period bodywave waveforms (Ekström, 1987; Honda and Seno, 1989). In this short report we present a new method to incorporate first motion polarity data with the centroid moment tensor (CMT) inversion of Dziewonski *et al.* (1981) and apply it to large shallow earthquakes which occurred in Ecuador.

On March 6, 1987, two major earthquakes with magnitudes $M_s = 6.1$ (1 : 54 GMT) and 6.9 (4 : 10) took place in northeastern Ecuador, along the eastern slopes of the Andes Mountains (Fig. 1). The mainshock is the largest subaerial earthquake that occurred in Ecuador in the last 90 years. The catastrophic mass wasting and flooding triggered by these earthquakes caused deaths of more than one thousand people and the severe destruction of the Trans-Ecuador oil pipeline; the estimated economic losses are one billion U.S. dollars (Nieto and Schuster, 1988). In Fig. 2, we compare the Harvard CMT (HCMT) solutions (Dziewonski *et al.*, 1988) with the P-wave first motion polarity data read from WWSSN long-period data for the three events. The HCMT solutions are usually very reliable, but there are some shallow events for which they are not reliable due to the above-mentioned problem (e.g., Kawakatsu, 1990). Here the HCMT solution for the foreshock is almost consistent with the first motion data, but those for the mainshock and aftershock have some discrepancies.

The P-wave first motion constraint for a moment tensor can be treated as a linear inequality constraint as follows (e.g., Tanimoto and Kanamori, 1986; Suetsugu and Nakanishi, 1988); for $j$-th station, the first motion P-wave amplitude is proportional to

$$\boldsymbol{g}_j(i, \phi) \cdot \boldsymbol{f}, \tag{1}$$

where $\boldsymbol{g}_j(i, \phi)$ can be calculated for a given set of ray direction parameters (i.e., a take-off angle $i$ and an azimuth $\phi$) and components of a vector $\boldsymbol{f}$ are the six independent elements

Received July 10, 1991; Accepted October 2, 1991

* To whom correspondence should be addressed.

** On leave from Department of Geological Sciences, Escuela Superior Politecnica del Litoral at Guayaquil, Ecuador.

PDE March 6-10, 1987

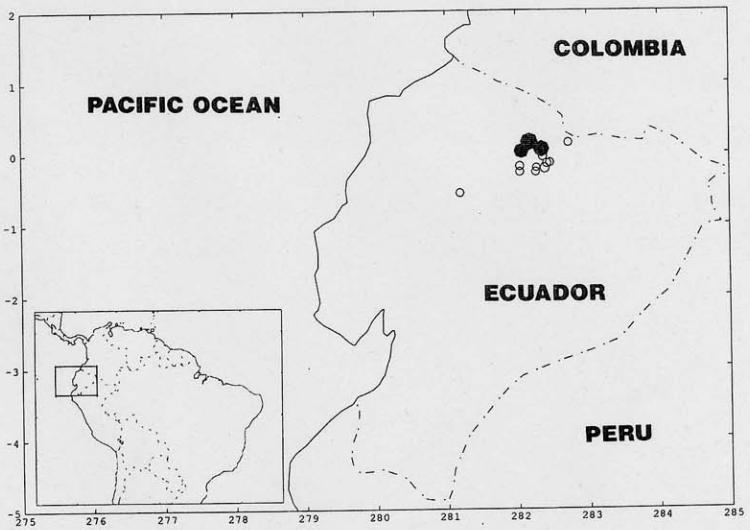


Fig. 1. The epicenters of shallow ( < 50 km) earthquakes which occurred in March 6–10, 1987, are shown. Closed marks indicate the three major events studied here.

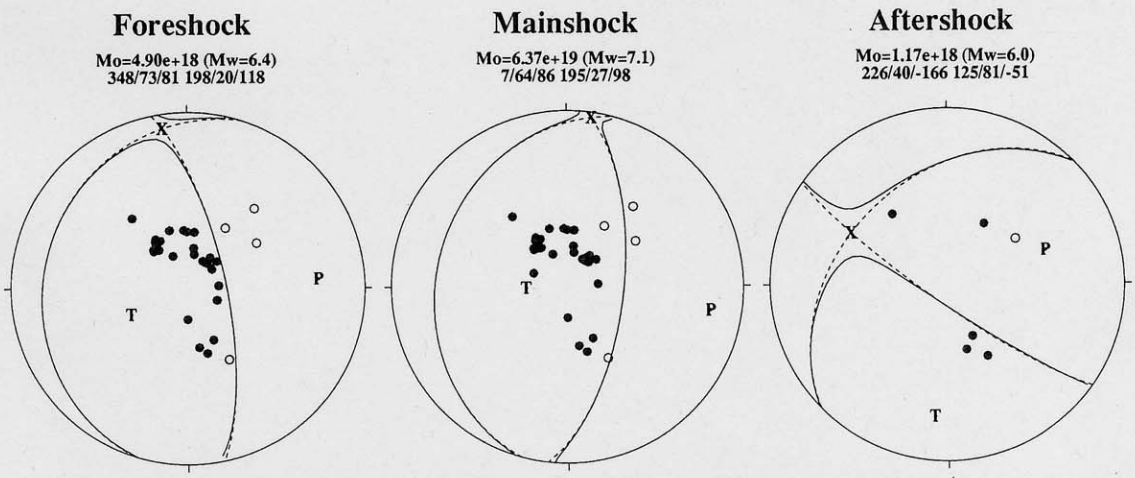


Fig. 2. The Harvard CMT solutions for the foreshock, the mainshock and the aftershock are plotted against the first motion polarity data obtained from WWSSN long-period records (equal-area projection of the lower hemispheres). The seismic moment in a unit of Nm and the nodal planes (strike/dip/slip) of the corresponding best double couples are given at the top of each plot.

of a moment tensor. Since (1) can be either positive or negative (unless the station is on the nodal plane) depending on the ray direction, the polarity constraint for a set of receivers may be expressed as the following inequality equations,

$$\boldsymbol{G}\cdot\boldsymbol{f}>0\,, \tag{2}$$

where each row of matrix $\boldsymbol{G}$ corresponds to $\boldsymbol{g}_j(i, \phi)$ multiplied by either $+1$ (positive polarity) or $-1$ (negative). In the present study, this inequality constraint, as well as the no-isotropic equality constraint, is incorporated with the standard CMT inversion procedure (Dziewonski *et al.*, 1981; Dziewonski and Woodhouse, 1983), using the "LSEI" program, which solves a linearly constrained least squares problem with both equality and inequality constraints (Lawson and Hanson, 1974; Hanson and Haskell, 1978, 1979).

In the CMT inversion, a moment tensor and centroid parameters (a hypocenter and an origin time) are determined by an iterative procedure. During each iteration, the inequality condition (2) may be modified as

$$\boldsymbol{G}\cdot(\boldsymbol{f}^{(0)}+\Delta\boldsymbol{f})>0\,, \tag{3}$$

where $\boldsymbol{f}^{(0)}$ is a moment tensor obtained in the previous iteration and $\Delta\boldsymbol{f}$ is the correction factor. In order to update the moment tensor, the inequality constraint which should be incorporated in the least squares procedure is then expressed as

$$\boldsymbol{G}\cdot\Delta\boldsymbol{f}>-\boldsymbol{G}\cdot\boldsymbol{f}^{(0)}\,. \tag{4}$$

Figure 3 and Table 1 summarize the results. P-wave first motion polarities are read from WWSSN long-period seismograms. Only those showing clear initial phases are used. P-wave velocity of 6 km/s is assumed to calculate take-off angles. For CMT inversions, long-period seismograms filtered between 3.5 and 7.0 mHz which contain the first minor-arc surface waves (R1 and G1) are used for the foreshock and mainshock; for the after shock, long-period bodywave seismograms (from the first P-wave arrival to just before an arrival of a first minor-arc surface wave) filtered between 12 and 20 mHz are used. Depths of centroid are all constrained to be 10 km.

The new CMT solutions for the March 6, 1987, earthquakes show the foreshock and mainshock have very similar mechanisms whereas the aftershock is an almost pure strike-slip fault. Seismic moments are somewhat reduced compared to those of the

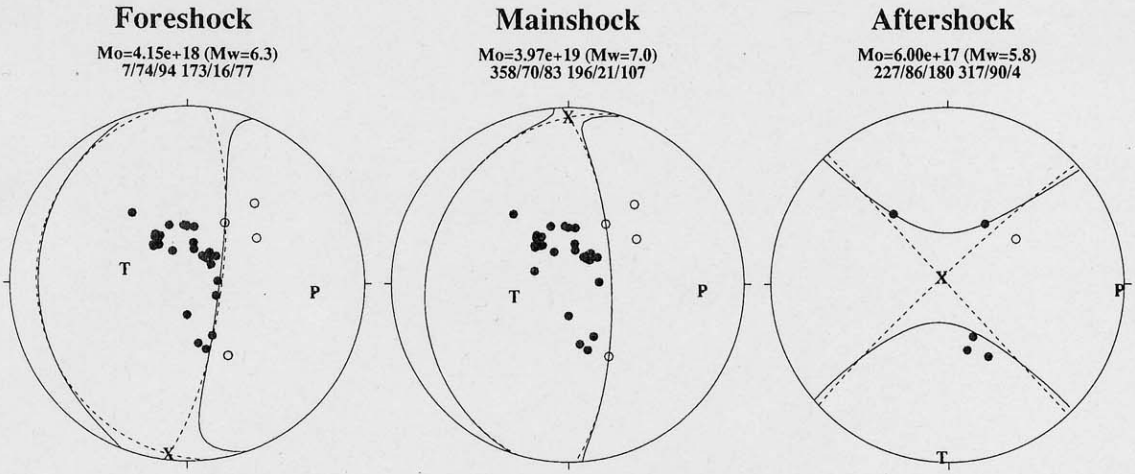


Fig. 3. Same as the Fig. 2 but for the new CMT solution. Note that now the first motion data are consistent with the moment tensor solutions.

Table 1. CMT solution.

| Foreshock | | | | | |
|---|---|---|---|---|---|
| PDE origin time 01:54:50.7 | | | | | |
| Centroid location | | | | | |
| origin time* | Latitude | Longitude | Depth (km) | | |
| $+7.3\pm2.0$ s | $0.19\pm0.13°$ | $282.81\pm0.11°$ | $10.0\pm0.0$ | | |
| Moment tensor | ($10^{18}$ N·m) | | | | |
| $M_{rr}$ | $M_{\theta\theta}$ | $M_{\phi\phi}$ | $M_{r\theta}$ | $M_{r\phi}$ | $M_{\theta\phi}$ |
| $2.03\pm0.12$ | $0.33\pm0.09$ | $-2.35\pm0.17$ | $0.48\pm0.75$ | $3.49\pm0.65$ | $-0.05\pm0.09$ |
| **Mainshock** | | | | | |
| PDE origin time 04:10:41.0 | | | | | |
| Centroid location | | | | | |
| origin time* | Latitude | Longitude | Depth (km) | | |
| $+10.9\pm0.9$ s | $0.09\pm0.06°$ | $282.63\pm0.03°$ | $10.0\pm0.0$ | | |
| Moment tensor | ($10^{19}$ N·m) | | | | |
| $M_{rr}$ | $M_{\theta\theta}$ | $M_{\phi\phi}$ | $M_{r\theta}$ | $M_{r\phi}$ | $M_{\theta\phi}$ |
| $2.52\pm0.08$ | $0.07\pm0.05$ | $-2.59\pm0.09$ | $-0.26\pm0.34$ | $3.00\pm0.27$ | $-0.33\pm0.05$ |
| **Aftershock** | | | | | |
| PDE origin time 08:14:48.5 | | | | | |
| Centroid location | | | | | |
| origin time* | Latitude | Longitude | Depth (km) | | |
| $+8.4\pm1.5$ s | $0.01\pm0.10°$ | $282.04\pm0.15°$ | $10.0\pm0.0$ | | |
| Moment tensor | ($10^{17}$ N·m) | | | | |
| $M_{rr}$ | $M_{\theta\theta}$ | $M_{\phi\phi}$ | $M_{r\theta}$ | $M_{r\phi}$ | $M_{\theta\phi}$ |
| $-0.90\pm0.88$ | $6.42\pm0.82$ | $-5.52\pm1.27$ | $-0.38\pm0.87$ | $0.25\pm0.71$ | $-0.47\pm0.45$ |

* Centroid time is relative to the PDE origin time.

HCMT solutions; this may partly be due to the differences in dip of nodal planes, assumed centroid depths and used earth models (we use 1066A of Gilbert and Dziewonski, 1975).

If an earthquake changes its focal mechanism during the faulting process, there is no reason why first motion data should be consistent with long-period waveform data. The assumption of a single focal mechanism is, therefore, implicit in the type of analysis presented in this report. In the absence of some strong evidence that an earthquake has a large non-double couple component or that it changes the fault plane during the rupture, we believe that the assumption is reasonable. The introduction of a first motion constraint sometimes greatly improves the stability of the CMT solution. The dip angles of the foreshock and the mainshock are very difficult to constrain from the type of data used here (Kanamori and Given, 1981), but with the presence of first motion constraints there exist no such difficulties.

We tried to constrain depths of the foreshock and mainshock by comparing first

motion P-wave waveforms with synthetics calculated by Nábělek's program (Nábělek, 1984). The procedure is the same as the one performed in Honda *et al.* (1990); the focal mechanism is fixed and only a source time function is deconvolved for given depths. Long- and short-period P-wave data read from the GDSN CD-ROM are converted into waveforms with WWSSN long-period response. Since no information is available for the crustal structure, we use a half space with P-wave velocity of 6 km.

Figure 4 shows the residual of the waveform fit and the estimated seismic moment as a function of a depth. For the foreshock, the residuals increase rapidly below a depth of 9 km and the centroid depth is thus estimated to be shallower than 9 km. The centroid depth of 5.3 km gives a seismic moment very similar to that of the CMT solution.

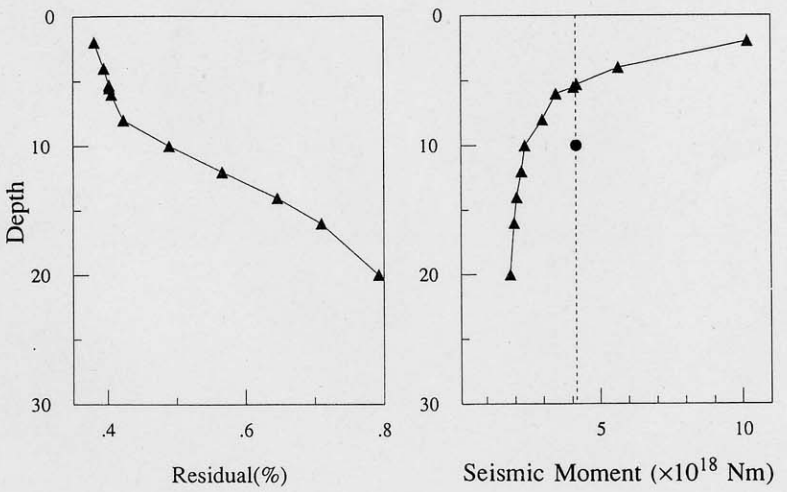


(a)

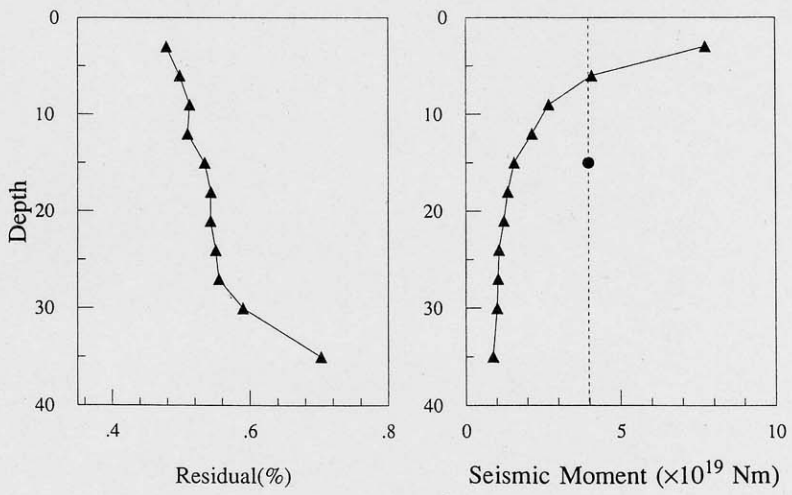


(b)

Fig. 4. Fit of P-wave first motion waveforms. Closed circles and broken lines indicate the seismic moments of the CMT solutions; (a) foreshock and (b) mainshock.

Allowing 50% error in the estimation of the seismic moment, the centroid depth is estimated to be between 4 and 9 km. The centroid depth of the mainshock is harder to estimate from this type of a simple analysis, because of the large size of the earthquake. From the waveform fit residuals (Fig. 4(b)), we can only say for sure that the centroid is shallower than about 30 km. Although there is a slight increase of the residual around 12 km depth, it may not be significant. Using a similar line of argument given above, however, from the seismic moment estimates, we suggest the centroid depth to be between 4 and 12 km.

Figure 5 shows all the available source mechanism solutions, determined by this work, the Harvard group (e.g., Dziewonski *et al.*, 1981) and Suárez *et al.* (1983). An interesting point in this figure is the following. Along the Pacific coast, many large thrust earthquakes have been occurring at the subduction zone but where Carnegie Ridge is subducting, no earthquake large enough to determine the source mechanism is present. "No known great earthquakes" is also reported in this area (Kelleher and McCann, 1976). In the sub-Andes region directly east of where Carnegie Ridge is subducting, on the other hand, there exist a high activity of earthquakes whose compressional axes are in the direction of an east-west horizontal (i.e., the direction of

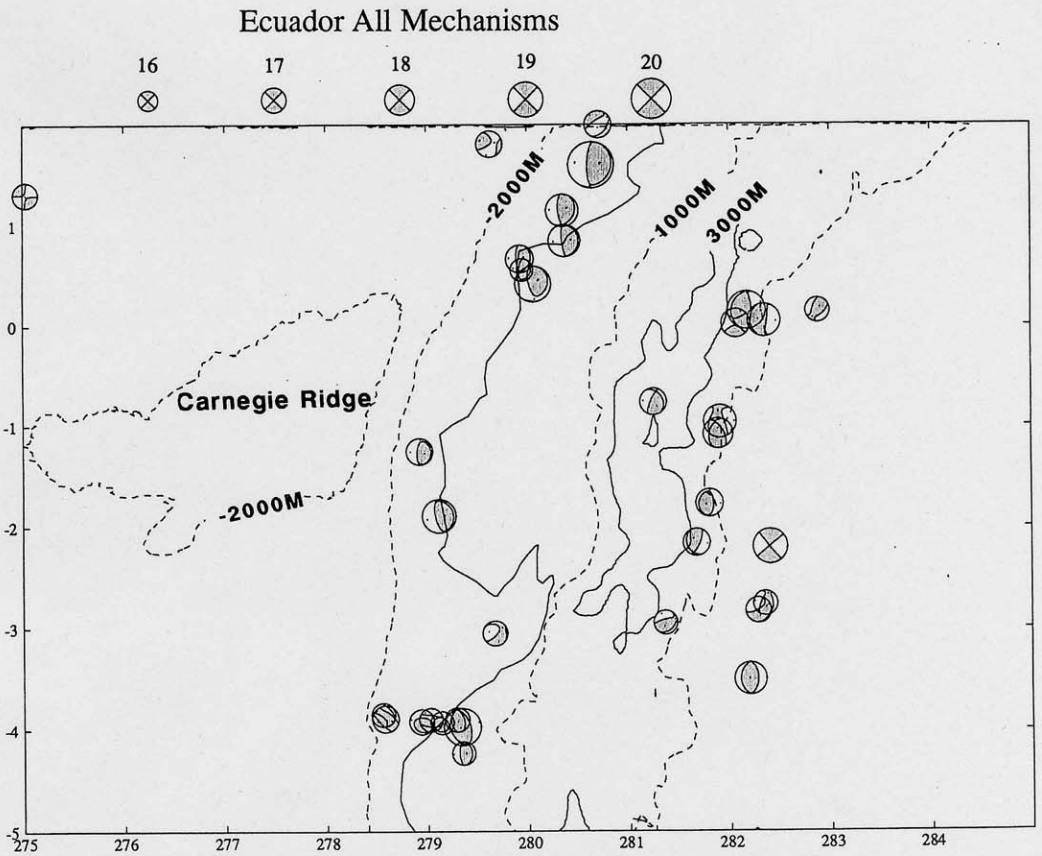


Fig. 5. All the available focal mechanisms (1963–1989) are plotted in their lower hemispheres. The size of each focal mechanism plot is proportional to the logarithm of the seismic moment.

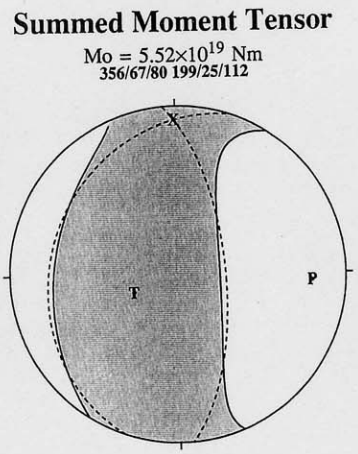


Fig. 6. Moment tensors of the 14 earthquakes which occurred in the sub-Andean region are summed. The summed moment tensor represents the overall seismic strain release in 27-year period in the Ecuadorian sub-Andes.

Table 2. Summed moment tensor for Ecuadorian sub-Andes.

| Moment tensor | ($10^{19}$ N·m) | | | | |
|---|---|---|---|---|---|
| $M_{rr}$ | $M_{\theta\theta}$ | $M_{\phi\phi}$ | $M_{r\theta}$ | $M_{r\phi}$ | $M_{\theta\phi}$ |
| 3.41 | 1.24 | −4.64 | −0.39 | 3.70 | −0.54 |
| Principal axes | | | | | |
| | *T*-axis | *N*-axis | *P*-axis | | |
| Moment | 4.94 | 1.17 | −6.10 | | |
| Plunge | 66.8 | 9.1 | 21.1 | | |
| Azimuth | 247.6 | 359.5 | 93.0 | | |

the plate convergence). It is, therefore, easy to postulate that the difficulty of releasing the compressional strain at the subduction thrust zone, due to the presence of "buoyant" Carnegie Ridge, resulted in the seismic strain release along the sub-Andean thrust belt, where crustal shortening might have been taking place in some geologic time (Suárez *et al.*, 1983) and thus a weak zone has been present. It should be also noted that the altitude of the Andes in this area is higher than the surrounding vicinities (see the 3,000 m high altitude contour line in Fig. 5).

Following Suárez *et al.* (1983), we can estimate the seismic crustal shortening rate by summing the moment tensor solutions in the area. Figure 6 and Table 2 show the summed moment tensor of 14 sub-Andean earthquakes. In order to calculate the deformed volume, we assumed 500 km in length and 250 km in width. As the thickness of the seismogenic zone we take a value of 15 km, although Suárez *et al.* (1983) use 40 km. The principal value of compressional seismic strain rate is estimated $1.2 \times 10^{-8}$ year$^{-1}$ and comparable to that of the "Central Andes" estimated by Suárez *et al.* (1983) (although our value of the strain rate is larger, because of the assumed thinner seismogenic zone, the actual seismic activity is in the same order; i.e., if we used the thickness of 40 km, the strain rate would be $4.4 \times 10^{-9}$ year$^{-1}$). Since the seismic moment

of the March 6 mainshock takes up over 70% of the summed moment, without any known recurrence interval, we believe that the estimated seismic strain rate should be considered as the maximum value. Suárez *et al.* (1983) suggested that if that level of seismic shortening has been occurring in some geologic time (about the last 100 m.y.), it is possible to explain the presence of the Andes by such a tectonic shortening without requiring some other mechanisms. The presence of the relatively high altitude in the Ecuadorian Andes may be a result of such tectonic crustal shortening accelerated in the recent geologic time due to the subduction of the Carnegie Ridge.

This research was conducted as a part of the individual traing course provide by Japan International Cooperation Agency (JICA) and IISEE of Building Research Institute. One of the authors (GPC) thanks for their support. We also thank Mr. Shingo Watada of Caltech for kindly supplying us the GDSN data, and Dr. Tetsuzo Seno and Dr. Masanori Saito for valuable comments on the manuscript.

## REFERENCES

Dziewonski, A. M. and J. H. Woodhouse, An experiment in the systematic study of global seismicity: Centroid-moment tensor solutions for 201 moderate and large earthquakes of 1981, *J. Geophys. Res.*, **88**, 3247–3271, 1983.

Dziewonski, A. M., T.-A. Chou, and J. H. Woodhouse, Determination of earthquake source parameters from waveform data for studies of global and regional seismicity, *J. Geophys. Res.*, **86**, 2825–2853, 1981.

Dziewonski, A. M., G. Ekström, J. H. Woodhouse, and G. Zwart, Centroid-moment tensor solutions for January–March 1987, *Phys. Earth Planet. Inter.*, **50**, 116–126, 1988.

Ekström, G., A broad band method of earthquake analysis, Ph. D. thesis, Harvard University, 1987.

Gilbert, F. and A. M. Dziewonski, An application of normal mode theory to the retrieval of structural parameters and source mechanisms from seismic spectra, *Philos. Trans. R. Soc. London, Ser. A*, **278**, 187–269, 1975.

Hanson, R. J. and K. H. Haskell, Sandia Laboratories Technical Reports, Sand77-0552, 1978.

Hanson, R. J. and K. H. Haskell, Sandia Laboratories Technical Reports, Sand78-1290, 1979.

Honda, S. and T. Seno, Seismic moment tensors and source depths determined by the simultaneous inversion of body and surface waves, *Phys. Earth Planet. Inter.*, **57**, 311–329, 1989.

Honda, S., H. Kawakatsu, and T. Seno, The depth of the October 1981 off Chile outer-rise earthquake ($M_s$=7.2) estimated by a comparison of several waveform inversion methods, *Bull. Seismol. Soc. Am.*, **80**, 69–87, 1990.

Kanamori, H. and J. W. Given, Use of long-period surface waves for rapid determination of earthquake source parameters, *Phys. Earth Planet. Inter.*, **27**, 8–31, 1981.

Kawakatsu, H., CMT solution of the Izu-Oshima-Kinkai earthquake of January 14, 1978, *Zisin*, **43**, 447–450, 1990 (in Japanese).

Kelleher, J. and W. McCann, Buoyant zones, great earthquakes and unstable boundaries of subduction, *J. Geophys. Res.*, **81**, 4885–4896, 1976.

Lawson, C. L. and R. J. Hanson, *Solving Least Squares Problems*, Prentice-Hall, Englewood Cliffs, N. J., 340 pp., 1974.

Michael, A. and R. J. Geller, Linear moment tensor inversion for shallow thrust earthquakes combining first-motion and surface wave data, *J. Geophys. Res.*, **89**, 1889–1897, 1984.

Nábělek, J. L., Determination of earthquake source parameters from inversion of body waves, Ph. D. thesis, Massachusetts Institute of Technology, 1984.

Nakanishi, I. and H. Kanamori, Source mechanisms of twenty-six large shallow earthquakes $M_s > 6.5$ during 1980 from P-wave first motion and long-period Rayleigh wave data, *Bull. Seismol. Soc. Am.*, **74**, 805–818, 1984.

Nieto, A. S. and R. L. Schuster, Mass wasting and flooding induces by the 5 March 1987 Ecuador Earthquakes, *Landslide News*, **2**, 5–8, 1988.

Suárez, G., P. Molnar, and B. C. Burchfiel, Seismicity, fault plane solutions, depth of faulting, and active tectonics of the Andes of Peru, Ecuador, and southern Colombia, *J. Geophys. Res.*, **88**, 10403–10428, 1983.

Suetsugu, D. and I. Nakanishi, Re-examination of fault model for the 1982 Urakawa-oki earthquake by analyses of seismic, geodetic, and Tsunami data, *J. Phys. Earth*, **36**, 53–67, 1988.

Tanimoto, T. and H. Kanamori, Linear programming approach to moment tensor inversion of earthquake sources and some tests on the three-dimensional structure of the upper mantle, *Geophys. J. R. Astron. Soc.*, **84**, 413–430, 1986.